Monitoring Drake Passage with elephant seals: Frontal structures and snapshots of transport

L. Boehme[1]
NERC Sea Mammal Research Unit, University of St. Andrews, St. Andrews KY16 8LB, United Kingdom; British Antarctic Survey, Natural Environment Research Council, High Cross, Madingley Road, Cambridge CB3 0ET, United Kingdom

S. E. Thorpe
British Antarctic Survey, Natural Environment Research Council, High Cross, Madingley Road, Cambridge CB3 0ET, United Kingdom

M. Biuw and M. Fedak
NERC Sea Mammal Research Unit, University of St. Andrews, St. Andrews KY16 8LB, United Kingdom

M. P. Meredith
British Antarctic Survey, Natural Environment Research Council, High Cross, Madingley Road, Cambridge CB3 0ET, United Kingdom

Abstract

Conductivity–temperature–pressure satellite relay data loggers (CTD-SRDLs) were attached to southern elephant seals (*Mirounga leonina*) on the island of South Georgia. During the animals' migration the CTD-SRDLs recorded and transmitted hydrographic profiles at a rate of approximately two profiles per day to an average depth of about 547 m, representing transect-type sections with a spatial resolution of 16–47 km along the migratory routes of the seals. Two sections are used to clearly identify the locations of the Antarctic Circumpolar Current fronts across Drake Passage, providing in situ data complementary to satellite and other techniques. An empirical relationship between upper ocean temperature and baroclinic mass transport is used to determine the transport through Drake Passage at the times of the sections, and these transports are compared with estimates derived by other techniques. An absolute geostrophic velocity section across Drake Passage is calculated using CTD-SRDL data and data of absolute geostrophic surface velocities from altimetry. The mean total baroclinic transports in June 2004 and April 2005 are estimated to be $124 \times 10^6 \pm 14 \times 10^6$ m^3 s^{-1} and $112 \times 10^6 \pm 14 \times 10^6$ m^3 s^{-1} respectively.

The Antarctic Circumpolar Current (ACC) dominates the horizontal circulation of the circumpolar Southern Ocean, and is a key component of the global ocean overturning circulation (Rintoul et al. 2001). The clockwise circulation around the Antarctic continent provides a vital link for transporting heat and freshwater between the Atlantic, Indian, and Pacific oceans. The transport of the ACC and its variability are therefore of considerable importance because of their influence on climate and ecosystem processes over large areas. With increasing expectations for predictions at increasingly fine resolutions, models must become more sophisticated, and the need for detailed in situ observations has never been more acute and is accelerating. Data are needed from regions and seasons where traditional hydrographic data (e.g., ship-based measurements, Argo floats, etc.) are scarce or difficult and expensive to implement. New approaches are being developed to fill this gap.

The flow of the ACC is not spatially uniform, with zones of relatively uniform water mass properties separated by narrow, deep-reaching current cores associated with the ACC fronts (Nowlin et al. 1977; Nowlin and Clifford 1982; Nowlin and Klinck 1986). Before these narrow fronts were fully resolved, estimated net transports of the ACC in Drake Passage ranged unrealistically widely, from 236×10^6 m^3 s^{-1} to -15×10^6 m^3 s^{-1}, because of coarse spatial and temporal sampling and inappropriate assumptions in transport calculations (Reid and Nowlin 1971; Foster

[1] Corresponding author (lb284@st-andrews.ac.uk).

Acknowledgments

We thank K. Bennett, C. Duck, I. Field, and S. Moss for their help on deploying satellite relay data loggers on South Georgia. A special thanks to the staff and engineers of Valeport Ltd. for their help in designing the oceanographic sensors for the Sea Mammal Research Unit. The altimeter products were produced by the data unification and altimeter combination system as part of the segment sol multimissions d'altimétrie, d'orbitographie, et de localisation précise processing system and distributed by Aviso with support from the Centre National d'Études Spatiales. We thank the two anonymous reviewers for their helpful comments.

This research was funded by the Natural Environment Research Council (NERC) grant NER/D/S/2002/00426 and a NERC Co-operative Award in Science & Engineering Ph.D. studentship supported by the Sea Mammal Research Unit Instrumentation Group of the University of St. Andrews and the British Antarctic Survey.

1972). Subsequently, repeat hydrographic measurements were made as early as the mid 1970s as part of the International Southern Ocean Studies (ISOS) experiment. ISOS fully revealed the banded structure of the ACC, and derived a mean transport of $134 \times 10^6 \pm 13 \times 10^6$ m^3 s^{-1} using the repeat hydrography and moorings data (Whitworth 1983; Whitworth and Peterson 1985).

Whitworth and Peterson (1985) suggested that the ACC is in geostrophic balance and concluded that although about three-quarters of the net transport is in the baroclinic component, transport variability is mainly barotropic on timescales up to around annual. Reanalysis of the ISOS moorings data led Cunningham et al. (2003) to argue that the barotropic and baroclinic variability in Drake Passage transport are comparable even on subseasonal timescales. More recent analyses have demonstrated that barotropic variability dominates the transport through Drake Passage on timescales up to around seasonal, with baroclinic variability becoming important at annual and interannual timescales (Hughes et al. 2003; Meredith et al. 2004).

Annual occupations of a repeat hydrographic section (WOCE SR1) began in 1993 during the World Ocean Circulation Experiment (WOCE). Cunningham et al. (2003) estimated the baroclinic transport to be $136.7 \times 10^6 \pm 7.8 \times 10^6$ m^3 s^{-1} from six SR1 hydrographic sections and reanalyzed the ISOS data and found the uncertainty of the mean net transport to be around 35×10^6 m^3 s^{-1}, significantly larger than suggested by Whitworth and Peterson (1985). Cunningham et al. (2003) and Sprintall (2003) observed the two northernmost fronts of the ACC to be highly variable, meandering on interannual timescales. This interannual frontal variability was confirmed by Boehme et al. (in press), showing the high variability of the Polar Front (PF) in Drake Passage on subannual timescales.

Today it is known that the circumpolar transport variability of the ACC on timescales from days to years is forced by fluctuations in the Southern Annual Mode (SAM), the dominant extratropical mode of climate variability in the Southern Hemisphere (Thompson and Wallace 2000). Despite a trend toward a higher-index state in recent decades, the SAM is strongly modulated by season (Thompson and Solomon 2002). The range in transports shown by the ACC on interannual timescales is seen to be rather small, however, and this is believed to be due to energy being cascaded to smaller (mesoscale) length scales via baroclinic instability (Meredith and Hogg 2006). Equally importantly, Meredith et al. (2004) showed that the interannual changes in the seasonal signal in the SAM are reflected in changes in the seasonal signal in the ACC transport.

Repeat hydrographic and expendable bathythermograph (XBT) sections are continuing (e.g., Sprintall 2003; Sokolov et al. 2004), but these measurements alone are not adequate for monitoring the interannual variability in the ACC transport, or changes to the seasonal signal in ACC transport due to changes in the SAM (Meredith and Hughes 2005). Such estimates are hugely aliased by short-term variability, e.g., eddies and higher-frequency transport changes. High-frequency variability in Drake Passage can produce aliased signals even with a 10-d altimeter sampling (Gille and Hughes 2001). Meredith and Hughes (2005) showed that sampling intervals very much shorter than 10 d are needed.

Although estimates of ACC transport variability on interannual timescales that derive from ship-based repeat hydrographic and XBT sections data are badly aliased (Meredith and Hughes 2005), it remains open to question whether such data are capable on longer timescales (decadal) of monitoring changes in transport. The key would be to have a sufficient number of occupations so that the estimated mean for a given period would be a robust indicator of the actual mean, against the background of inherent variability at higher frequencies. If this approach were to work, it is likely that a very large number of sections across Drake Passage would be needed, i.e., more than are currently obtainable with research ships. Another problem is the seasonal variability in the ACC transport (Meredith et al. 2004). Conductivity–temperature–depth (CTD) and XBT sections are conducted almost entirely in the austral summer; thus any estimates of mean transport on the basis of these sections will be potentially biased.

Alternative approaches are proxy techniques based on less expensive measurements that can be obtained more frequently, also from the austral winter, and do not require research vessels (Lydersen et al. 2002). Here we present a new set of underway observations from Drake Passage and show their usefulness in identifying and pinpointing ACC frontal features. Although not preplanned, we show that the new technique of "adaptive-sampling" results in higher resolution at the ACC fronts. We demonstrate further that these measurements have comparable utility to XBT and expendable CTD (XCTD) sections for studies seeking to monitor ACC transport variability. By including winter-time data into such efforts, we will help alleviate some of the problems with aliasing at interannual periods. At longer periods these new data may help define more robust transport means, if sustained over several decades.

Data

Hydrographic data—Within the framework of the international SEaOS project (southern elephant seals as oceanographic samplers), 21 southern elephant seals (*Mirounga leonina*) on South Georgia were equipped with CTD satellite relay data loggers (CTD-SRDLs). This interdisciplinary program is aimed at increasing our understanding of how southern elephant seals interact with their physical environment (Biuw et al. 2007) and also at demonstrating and implementing this cost-effective means of gathering routine observations of hydrographic data from remote environments (Boehme et al. in press). CTD-SRDLs, custom built by the Sea Mammal Research Unit, St. Andrews, United Kingdom and Valeport Ltd., Devon, United Kingdom, were fixed harmlessly to seals' fur after the elephant seals completed their annual molt in January and February and were finally lost when the animals molted again the following season. During the animals' migration, the CTD-SRDLs report vertical profiles of

salinity, temperature, and pressure to a depth of up to 2,000 m with an accuracy of better than 0.02 in temperature and salinity (Boehme et al. in press), hence of at least same quality as XBT/XCTD data (Boyd and Linzell 1993).

Several animals traveled west from South Georgia toward the Antarctic Peninsula and two crossed Drake Passage nearly perpendicular to the flow (Fig. 1). Here we show two hydrographic sections obtained by the southern elephant seals Rudolph and Jason in 2004 and 2005 (Fig. 1). Rudolph crossed the western Drake Passage between 07 June 2004 and 20 June 2004 from the Antarctic Peninsula toward the western side of Burdwood Bank. He sampled 96 temperature profiles with an average station spacing of 16 km, an average profile depth of 469 m, and a range of profile depths between 118 m and 1,000 m (Fig. 2). Between 01 April 2005 and 15 April 2005, Jason traveled from Elephant Island to the southeastern side of Burdwood Bank very close to the WOCE repeat section SR1b. Eighteen CTD profiles were recorded with an average station spacing of 47 km and profile depth of 624 m, with a profile depth range from 260 m to 1,074 m (Fig. 3). The CTD-SRDL configuration was set to ensure batteries lasted until seals return to breed in September and only one CTD profile was sampled every 6 h. However, the horizontal spacing of consecutive dives deeper than 200 m (without sampling a CTD profile) is less than 6 km on average for both animals. Hence, the configuration could be optimized in the future to increase the spatial and temporal resolution of such hydrographic sections made by southern elephant seals.

Absolute dynamic topography—We use the maps of absolute dynamic topography product (MADT) of the data unification and altimeter combination system (DUACS), which is part of the multimission ground segment of the Centre National d'Études Spatiales. This system processes Jason-1, Envisat, GFO, ERS-1, ERS-2, and Topex-Poseidon altimeter data and synchronizes it with auxiliary data. Each mission is homogenized using the same models and corrections. A multimission cross-calibration process removes any residual orbit error, or long wavelength error, as well as large-scale biases and discrepancies between various data flows (SSALTO/DUACS User Handbook 2006). All altimeter fields are interpolated at crossover locations and dates. After a repeat-track analysis, a mean profile is subtracted to compute sea level anomaly. Data are then cross-validated, filtered from residual noise and small scale signals, and finally subsampled to give the sea level anomaly (SLA) product. Absolute dynamic topography (ADT) products are obtained by computing ADT = SLA + mean dynamic topography (MDT) (Rio and Hernandez 2004). The final mapping procedure generates a combined map merging measurements from all available altimeter missions. Geostrophic velocity maps are computed using finite differences. The MADTs have global coverage and include ADT and the corresponding geostrophic velocities on a third-degree Mercator grid (SSALTO/DUACS User Handbook 2006).

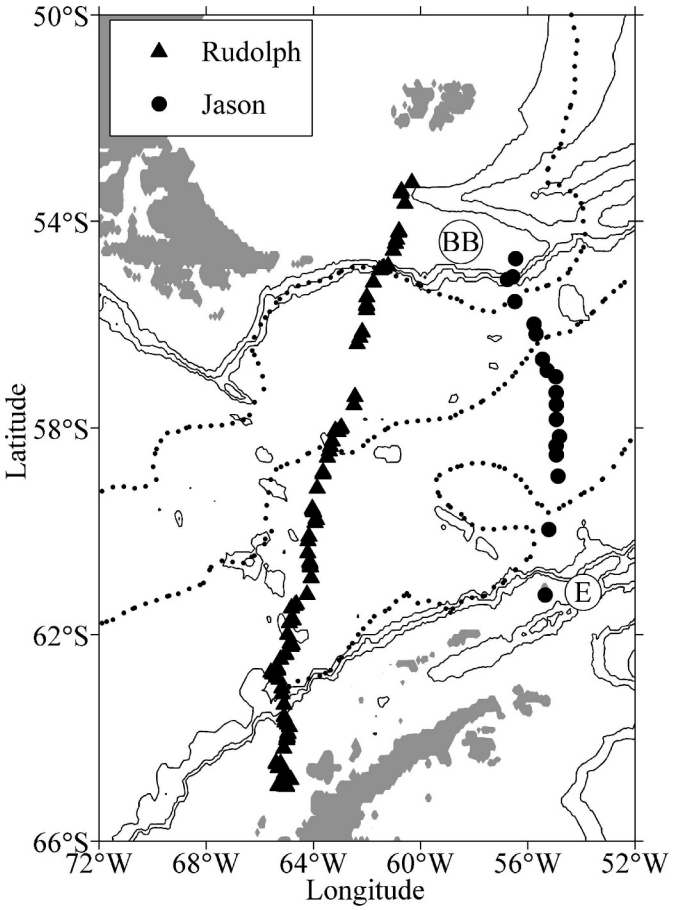

Fig. 1. The positions of the CTD-SRDL hydrographic profiles from Rudolph (triangles) and Jason (circles) sampled 07–20 June 2004 and 01–15 April 2005 respectively. The mean position for 2004 and 2005 of the Subantarctic Front, Polar Front, and southern ACC Front (from north to south) by Boehme et al. (in press) are shown as dotted lines. Burdwood Bank (BB) and Elephant Island (E) are marked. Isobaths are 1,000 m, 2,000 m, and 3,000 m and land is shaded gray.

Results

Frontal structures in Drake Passage—Rudolph was equipped with a temperature-only SRDL and the data are shown in Fig. 2. There is no clear near-surface temperature minimum layer visible, indicating winter conditions along the entire section. As typically seen in meridional sections across the ACC, the temperature decreases to the south in a series of steps or fronts, separated by zones of weaker meridional gradients. Although this winter section shows clear horizontal temperature gradients, which are associated with the Subantarctic Front (SAF) at about 55°S very close to the Burdwood Bank and the PF at about 58°S, the southern ACC Front (SACCF) close to the continental shelf at about 63°S is less pronounced. Between the PF and the SAF lies a zone of nearly homogeneous water without a pronounced thermocline. Of great interest, and potentially great usefulness, is the fact that Rudolph spent more time

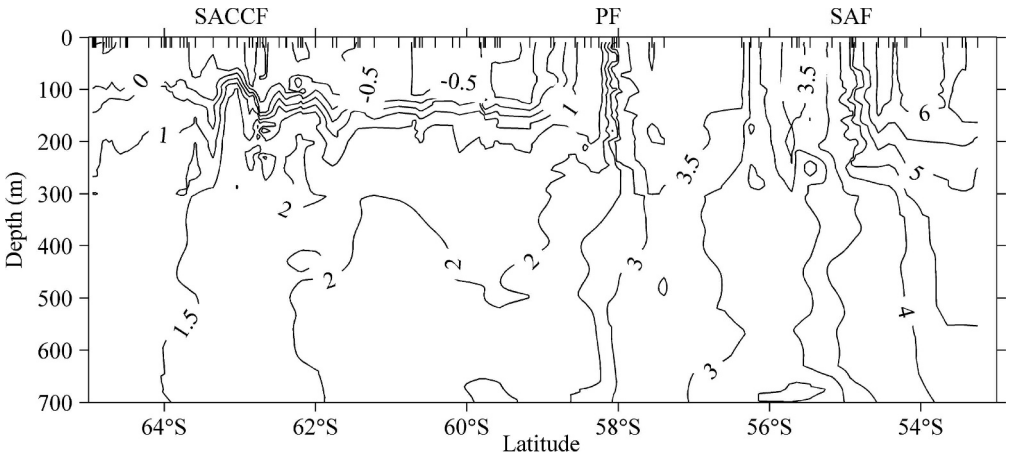

Fig. 2. In situ temperature section sampled by Rudolph. The positions of the profiles are given on the top axis to show the horizontal resolution of the temperature data. Front locations are marked on the upper axis. SACCF, southern ACC Front; PF, Polar Front; and SAF, Subantarctic Front.

close to the fronts, which can be seen in the closer station spacing (Fig. 2).

About a year later, Jason recorded a full CTD transect across the Drake Passage further to the east at the end of the austral summer (Fig. 3). The temperature minimum layer between 100 m and 200 m depth is still visible. The first profile of the section at 61°S is on the Antarctic Shelf to the southwest of Elephant Island. These shelf waters are indicated by a warmer surface layer of more than 2°C south of 60°S. Further north the higher salinities of the Circumpolar Deep Water (CDW) become apparent below 300 m depth, and further north still the relatively horizontal isotherms and isohalines get distorted by the strong current cores and eddies within the ACC (Fig. 3). Orsi et al. (1995) defined the SACCF as the southernmost eastward core of the ACC that carries waters with circumpolar characteristics, which is distinct from the Antarctic regime farther south. Using this definition and the vertical isotherms locates the SACCF at about 59°S. The surface expression of the PF is clearly marked by the increase of the sea surface temperature from 2.5°C to 5°C at about 57°S.

Between 57°S and 56°S there is a cold extension of water descending from south to north (Fig. 3). Figure 4 shows the potential temperature (Θ) versus salinity relationships for this section by Jason. The low temperature and salinity immediately identifies it as being derived from the temperature minimum layer, i.e., winter water, with a potential density of σ_Θ = 27.3 kg m^{-3}. It is of Antarctic origin with a depth of about 150 m south of the PF, and subducts to the north of the PF to intermediate depths of more than 500 m (Fig. 3). The SAF has again no strong surface expression, but is indicated by the vertical isotherms at 55°S close to Burdwood Bank.

Estimating transports from in situ temperature—Monitoring ocean transports requires measurements of the density field as well as changes in the pressure field associated with the barotropic flow. To calculate the geostrophic transport from only temperature sections it is necessary to first obtain a relationship between the steric height, relative to a specified reference level, and temperature (Sprintall 2003). In regions characterized by a single well-defined temperature–salinity (T-S) relationship, a mean T-S curve can be formulated using historical salinity data to identify the salinity corresponding to each temperature observation. Steric height is then estimated from this salinity and the temperature observation relative to their deepest common depth (e.g., McCarthy et al. 2000). However, this is complicated in the Southern Ocean. Inversions and frontal variability mean that at some locations the T-S relationship is not unique; hence one temperature can correspond to several salinity values. Nevertheless, the envelope of the T-S relations does not change much with time and each streamline can be associated with a particular T-S curve. This relationship between upper ocean temperatures to some known (determined) structure function of steric height, potential energy anomaly, or transport stream function has been used extensively in regions where there are only limited numbers of deep hydrographic stations but a copious quantity of temperature data (Rintoul et al. 1997; Sprintall 2003; Sokolov et al. 2004).

Most studies applying this technique to estimate the transport in Drake Passage use a reference level of 2,500 m, because it is the deepest depth that lies above the height of the mid-passage topography and also appears to be an appropriate reference depth as determined by the historical analysis of baroclinic transport in Drake Passage (Whitworth and Peterson 1985; Rintoul et al. 2002). Some studies used a simple relationship between the mass transport function and a single temperature variable. This could be the mass transport function regressed against a single temperature measurement (Ridgway and Godfrey 1994), dynamic height against the average temperature from the surface to 600 m (Rintoul et al. 1997), or the baroclinic transport stream function, $\chi_{2,500}$, against the averaged temperature (T_h) between 600 m and 700 m depth (Sokolov et al. 2004):

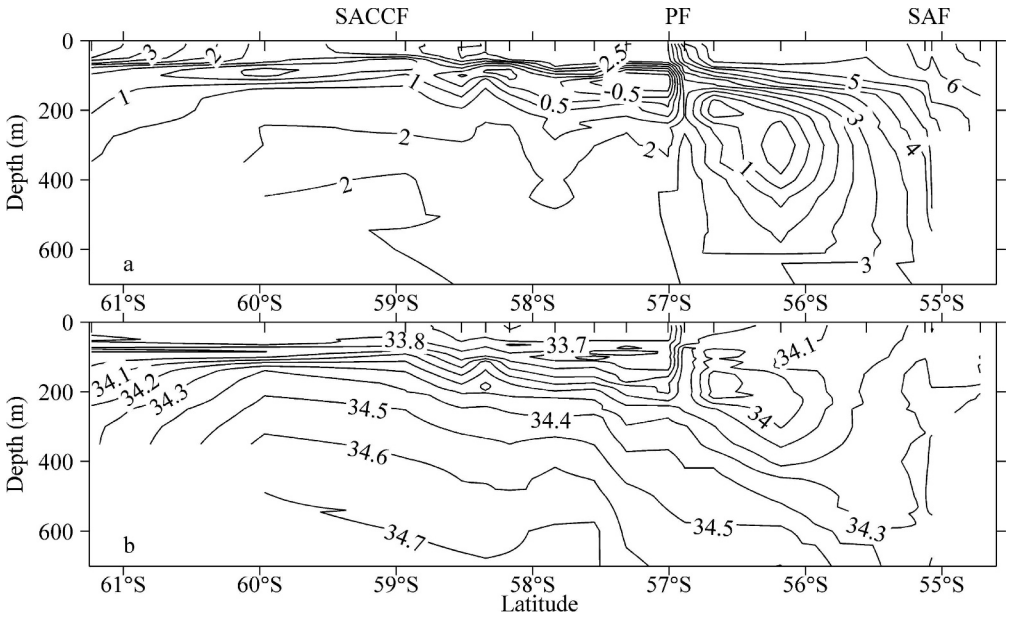

Fig. 3. (a) In situ temperature and (b) salinity sections made by Jason. The positions of the CTD profiles are given on the top axis to show the horizontal resolution of the temperature data. Front locations are marked on the upper axis. SACCF, southern ACC Front; PF, Polar Front; and SAF, Subantarctic Front.

$$\chi_{2,500} = \left(2.1024\overline{T_h}^7 - 26.815\overline{T_h}^6 + 138.81\overline{T_h}^5 - 385.31\overline{T_h}^4 + 641.27\overline{T_h}^3 - 643.39\overline{T_h}^2 + 360.61\overline{T_h} + 1.4552\right)\cdot 10^5 \quad (1)$$

The zonal transport per unit width, $U\chi$, is then (Sokolov et al. 2004):

$$U_\chi = -\frac{1}{\rho_{2,500} f}\frac{\partial}{\partial y}\chi_{2,500} \quad (2)$$

where $\rho_{2,500}$ is the reference density and f is the Coriolis parameter. Sprintall (2003) finds a relationship between the mass transport function, $Q_{2,500}$, and the temperatures at 100 m (T_{100}), 400 m (T_{400}), and 700 m (T_{700}):

$$Q_{2,500} = 47.25 + 4.76T_{100} - 2.54T_{400} + 28.47T_{700} \quad (3)$$

The transport per unit width, U_Q, is then estimated from the gradient of the mass transport function $Q_{2,500}$ multiplied by g/f, where g is the acceleration due to gravity (Sprintall, 2003).

Both relationships are used to calculate the transport from each temperature section in Figs. 2 and 3. The transports derived from the transect of Rudolph are shown in Fig. 5a. The transports derived from $Q_{2,500}$ include much more detail and suggest that small current cores and branches only affect the upper layer above 600 m depth. These are then only resolved by the method based on Sprintall (2003) by including temperatures at shallower depths, T_{100} in particular. Hence, the transports based on $\chi_{2,500}$ lack these details and deliver unrealistic high values close to the shelf at 54°S. However, both methods show similar results, by placing the current core of the SAF at 55°S. The main PF current core lies at 58.1°S. The PF seems to have several shallow cores to the south with transports up to 10×10^6 m^3 s^{-1} based on $Q_{2,500}$, whereas the transport based on $\chi_{2,500}$ shows only one main core of more than 10×10^6 m^3 s^{-1}. The SACCF shows again many current branches between 64°S and 62°S when derived from $Q_{2,500}$. The transports on the basis of $\chi_{2,500}$ show only one small core at 63.5°S. This richness in detail close to the fronts in both derived transports is only realistically feasible by using "adaptive samplers." Figure 2 shows the decreased station spacing close to the fronts, increasing the detail of the three ACC fronts in this transect.

Figure 5b shows the transports derived from the transect of Jason. Both methods show similar results, but lack the detail of Fig. 5a (this transect consists of only 15 deep profiles compared with 81 in Fig. 5a). Again, transports derived from $Q_{2,500}$ include much more detail and show two current cores of the PF, the northern one less pronounced in the transports derived from $\chi_{2,500}$. The SAF lies very close to the continental shelf (Fig. 3), and the calculated transports should be treated with caution in areas with less than 2,500 m water depth. However, both methods seem to resolve the SAF at the northern end of the transect. The PF is associated with a stronger current than the SAF, in contrast to the section the year before (Fig. 5a).

The cumulative transports integrated from Fig. 5 are shown in Fig. 6. Including different depths to represent different water masses and a shallow depth T_{100} to capture the seasonal changes in $Q_{2,500}$ seems to deliver much more detail than the transport derived from $\chi_{2,500}$. The cumulative transports of both methods derived from Rudolph's data set correlate very well. Here, the method based on $Q_{2,500}$ captures the SACCF, including a countercurrent just north of the SACCF (Fig. 5), whereas the method based on $\chi_{2,500}$ lacks this transport. South of 60°S, the temperature

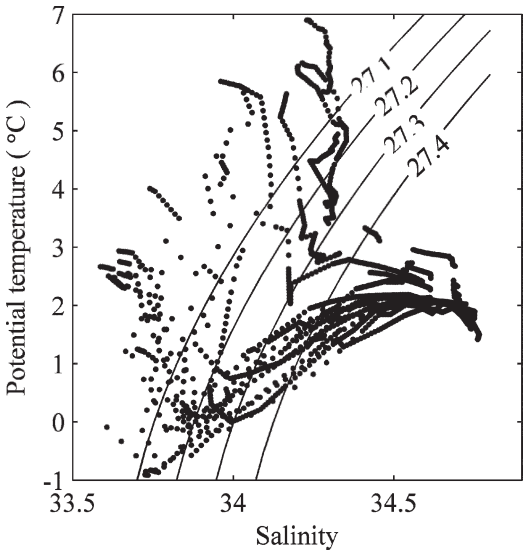

Fig. 4. Potential temperature versus salinity for the stations made by Jason. The σ_Θ = 27.3 kg m^{-3} isopycnal marks the approximate density of the Antarctic Intermediate Water of the Drake Passage.

corresponds to several salinity values and $\chi_{2,500}$ fails to resolve the different relationships between temperature and the stream function. However, $Q_{2,500}$ shows more detail in this region and seems to resolve the streamlines even close to the shelf at 64°S. The strongest current cores correlate well with the positions of the PF and SAF derived above (Fig. 2). Interestingly, both relationships show a decrease in transport between 57.5°S and 55.5°S between the two fronts and is due to the colder water below 200 m. Here, the two methods show a decline of about 20 × 10^6 m^3 s^{-1} (Fig. 6a) and a countercurrent just south of the SAF. Both relationships deliver estimates for the cumulative transports of 80 × 10^6 m^3 s^{-1} ($Q_{2,500}$) and 90 × 10^6 m^3 s^{-1} ($\chi_{2,500}$) above and relative to 2,500 m depth, with errors of ±11 × 10^6 m^3 s^{-1} ($Q_{2,500}$) and ±13 × 10^6 m^3 s^{-1} ($\chi_{2,500}$) respectively. These errors are due to the temperature accuracy and to the uncertainties in the empirical relationships $Q_{2,500}$ and $\chi_{2,500}$ (Sprintall 2003; Sokolov et al. 2004). Sokolov et al. (2004) showed that the transport of the upper 2,500 m accounts for about 67.6% ± 1.3% of the total baroclinic transport. Utilizing this number yields a total baroclinic transport of 118 × 10^6 m^3 s^{-1} ± 19 × 10^6 m^3 s^{-1} for the method based on $Q_{2,500}$ and 133 × 10^6 m^3 s^{-1} ± 22 × 10^6 m^3 s^{-1} for the method based on $\chi_{2,500}$ respectively. We then calculate the average of both estimates weighted by their variance, yielding a total baroclinic transport in June 2004 of 124 × 10^6 m^3 s^{-1} ± 14 × 10^6 m^3 s^{-1}.

The cumulative transports derived from the temperature transect of Jason are shown in Fig. 6b. This transport function further to the east in Drake Passage seems to lack small-scale features. Unfortunately, we have no deep stations between 59°S and the Antarctic continental shelf and therefore might underestimate the transport through Drake Passage by lacking the SACCF transport. The main current is associated with the PF (Fig. 5b); hence the biggest increase of the cumulative transport is around 57°S. The method based on $Q_{2,500}$ shows a weak countercurrent just south of the PF. As the SAF lies close to the continental shelf, the integrated data should be treated with care. The transports above and relative to 2,500 m are 70 × 10^6 m^3 s^{-1} ± 11 × 10^6 m^3 s^{-1} ($Q_{2,500}$) and 80 × 10^6 m^3 s^{-1} ± 13 × 10^6 m^3 s^{-1} ($\chi_{2,500}$). Again, utilizing the relationship between the transport in the upper 2,500 m

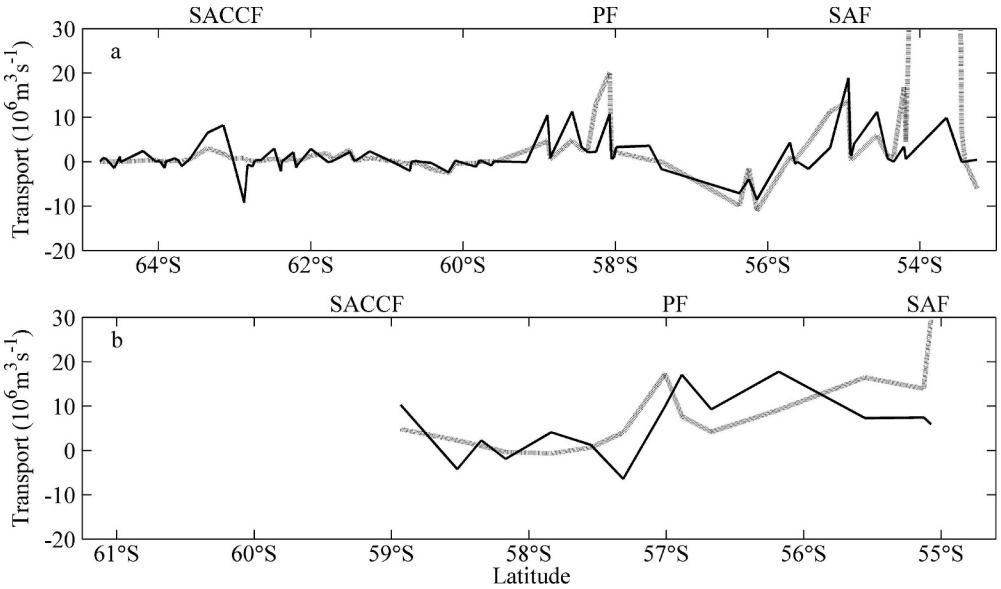

Fig. 5. The transport per unit width (10^6 m^3 s^{-1}) above 2,500 m depth derived from mass transport function $Q_{2,500}$, U_Q (solid line) and the baroclinic transport stream function $\chi_{2,500}$, U_χ (dotted line) for the Drake Passage transects of (a) Rudolph in June 2004 and (b) Jason in April 2005. Front locations are marked on the upper axis. SACCF, southern ACC Front; PF, Polar Front; and SAF, Subantarctic Front.

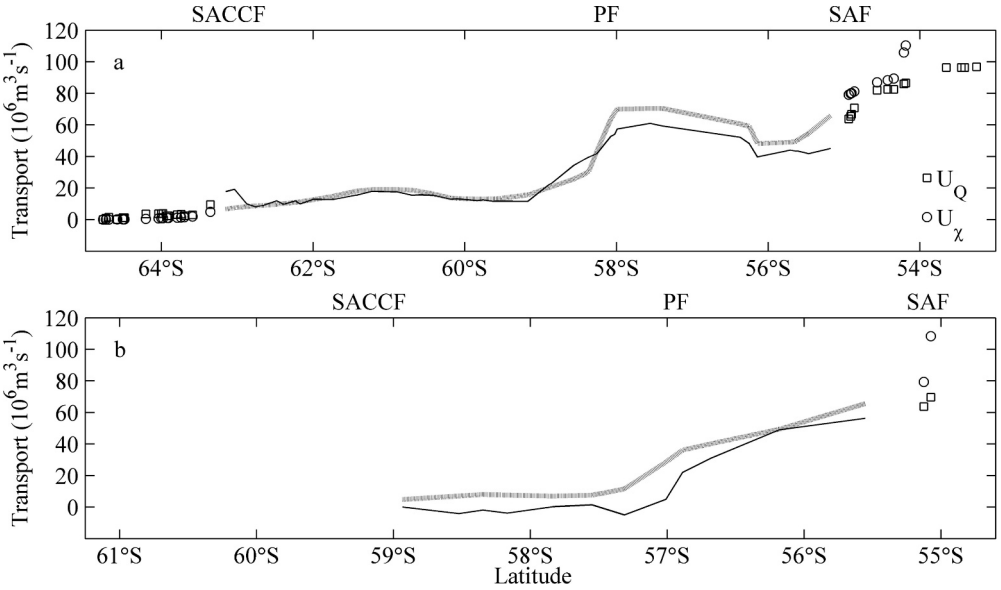

Fig. 6. Cumulative transport (10^6 m^3 s^{-1}) above 2,500 m depth derived from mass transport function $Q_{2,500}$, U_Q (solid line) and the baroclinic transport stream function $\chi_{2,500}$, U_χ (dotted line) for the Drake Passage transects of (a) Rudolph in June 2004 and (b) Jason in April 2005. The data are integrated from south to north, starting at the first profile with a water depth of more than 2,500 m. Data from positions with water depths of more than 2,500 m are lines, whereas others are marked with a circle and square. Front locations are marked on the upper axis. SACCF, southern ACC Front; PF, Polar Front; and SAF, Subantarctic Front.

and the total baroclinic transport of Sokolov et al. (2004) yields a total baroclinic transport of 104×10^6 m^3 s^{-1} $\pm$ 18×10^6 m^3 s^{-1} and 118×10^6 m^3 s^{-1} $\pm$ 22×10^6 m^3 s^{-1} respectively for the transect of Jason. The weighted average of both transports in April 2005 is 110×10^6 m^3 s^{-1} $\pm$ 14×10^6 m^3 s^{-1}.

Estimating transports from density—Although relatively inexpensive, CTD-SRDLs deliver not only temperature data, but also provide conductivity measurements to calculate salinity (Fig. 3). Hence, we can calculate density and the internal pressure field, from which the relative geostrophic currents relative to the surface are calculated. We took the corresponding surface geostrophic velocities closest in space and time from the MADT data set to derive a section of absolute geostrophic currents of the upper 1,000 m of Drake Passage (Fig. 7). The standard deviation of this velocity field is expected to be less than 0.1 m s^{-1} (Rio and Hernandez 2004).

Using the upper ocean temperature relationships ($Q_{2,500}$ and $\chi_{2,500}$) limits the data set to profiles that are at least 700 m deep. Here we are not limited to these deep profiles and can include shallower hydrographic profiles to extend our section further to the south and north, although we exclude profiles taken on the continental shelf. The flow can be seen to be ordered in vertically coherent, strong down-passage currents separated by much weaker mean currents (Fig. 7). All three fronts are correlated with such strong current cores. The SAF has a maximum velocity of more than 0.4 m s^{-1} just south of the position of the hydrographic front at 55°S. There is an indication of a stronger current core of more than 0.8 m s^{-1} below 400 m depth. Between the SAF and the PF lies a zone of eastward flow between 0.4 m s^{-1} and 0.6 m s^{-1}. The PF has two current cores at depth. The stronger one extends close to the surface north of the hydrographic-based position at 57°S with velocities higher than 0.6 m s^{-1}. Just south of the PF is a current core below 700 m depth with a maximum velocity of just over 0.4 m s^{-1}. Around 58.4°S lies a region with no flow to the east and a slowly westward-flowing current core below 100 m depth. At 59°S the SACCF is visible with an eastward current of up to 0.2 m s^{-1}, although because of the lack of deep profiles further south, we miss the maximum current core. Nevertheless, this frontal jet supports the position of the SACCF on the basis of the hydrographic data in Fig. 3. South of 59.5°S a westward-flowing current marks the southern limit of the ACC and the position of the Antarctic Slope Front. In calculating the cumulative transport (Fig. 6b), the southern limit to the section means that the transport of the SACCF is not taken into account (Fig. 7). This is evidence that we underestimate the total transport across Drake Passage in April 2005 derived from the mass transport function $Q_{2,500}$ and the baroclinic transport stream function $\chi_{2,500}$. The cumulative transport above 250 m depth is derived from the absolute geostrophic velocity section and shown in Fig. 7. The surface layer down to 250 m depth transports about 38×10^6 m^3 s^{-1} $\pm$ 15×10^6 m^3 s^{-1} to the east.

Discussion and summary

Frontal structures—Some definitions exist for determining the positions of the ACC fronts (Orsi et al. 1995; Belkin and Gordon 1996). Orsi et al. (1995) and Sprintall (2003) locate the SAF at the maximum subsurface temperature gradient between the 4°C and 5°C isotherms at 400 m depth, whereas Boehme et al. (in press) position the SAF at the 4°C isotherm at 300 m depth. Both definitions give very

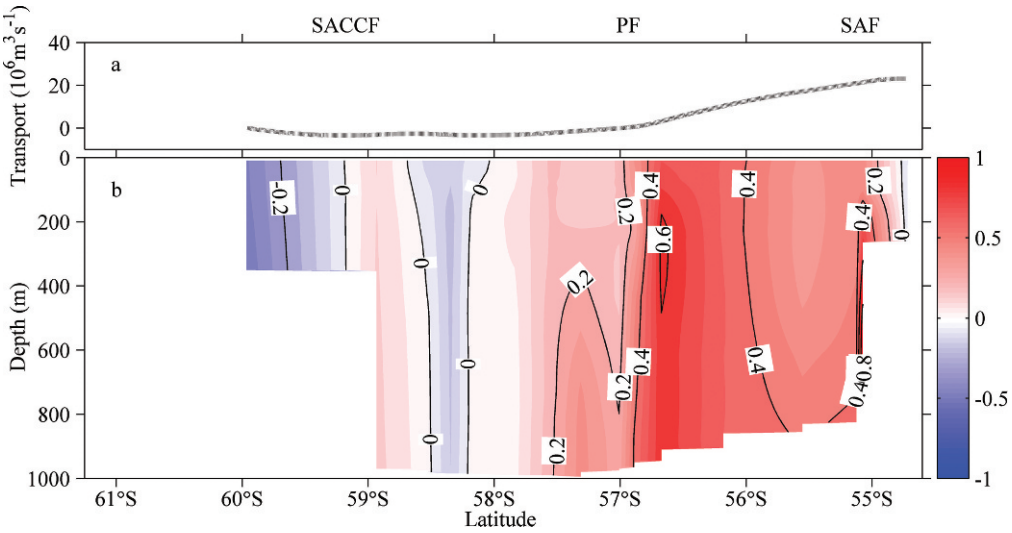

Fig. 7. (a) Cumulative transport (10^6 m^3 s^{-1}) (top) above 250 m depth (dotted line) derived from (b) absolute geostrophic velocities across the Drake Passage (m s^{-1}) at the beginning of April 2005. Hydrographic data of Jason are used to derive relative geostrophic velocities and then corrected by corresponding surface geostrophic velocities obtained from maps of absolute dynamic topography. Positive velocities are to the east. Front locations are marked on the upper axis. SACCF, southern ACC Front; PF, Polar Front, and SAF, Subantarctic Front.

close results when applied to the transect of Jason (Fig. 3). Very interesting is the wintertime occupation of Drake Passage by Rudolph (Fig. 2). Here, the definition of Orsi et al. (1995) would place the SAF incorrectly, whereas the definition of Boehme et al. (in press) is still valid. This discrepancy is due to the fact that wintertime data of Drake Passage, which contributed to the definition of the criterion of Boehme et al. (in press), are rare and therefore not well-represented in the study of Orsi et al. (1995). The position of the SAF correlates closely with the mean frontal positions of Boehme et al. (in press).

The PF is defined by the northernmost extent of the 2°C isotherm at 200 m depth (Orsi et al. 1995). This definition is also valid for the wintertime data in Fig. 2. The zone of nearly homogeneous water between the PF and the SAF can, however, blur this position. The position of the PF lies further north than the mean frontal position of Boehme et al. (in press). However, Boehme et al. (in press) show that the position of the PF in Drake Passage is accompanied by a strong variability.

The subducting winter water in Fig. 3 can also distort the position of the PF when using this simple criterion. Orsi et al. (1995) constrain their definition by including the crossing of the temperature minimum layer from above to below 200 m depth, which would position the PF at the correct place. Nevertheless, this crossing of Antarctic waters across the PF and its influence on intermediate waters north of the SAF supports the arguments of freshening of intermediate waters in the Subantarctic Zone by Antarctic waters (*see* Meredith et al. 1999 and references therein). This modified water will ultimately contribute to the fresh Antarctic Intermediate Water layer north of the ACC and imprint characteristics of Antarctic origin on those derived by deep convection north of the SAF (Piola and Gordon 1989; Talley 1996).

Orsi et al. (1995) place the SACCF at the location where the temperature maximum layer is below 500 m depth and above 1.8°C, whereas Boehme et al. (in press) apply a simple rule by selecting the 1.8°C isotherm at 500 m depth. Both these definitions give the same results when applied to the transect of Rudolph (Fig. 2). The transect of Jason does not show such a clear vertical 1.8°C isotherm. However, the 1.8°C isotherm of the temperature maximum layer crossing the 500 dbar isobar and the current cores of Fig. 7 support the position of the SACCF at 59°S, which again agrees well with Boehme et al. (in press).

Remotely sensed sea surface temperature (SST) data are often used to determine the positions of the SAF and PF within the ACC (Moore et al. 1999; Dong et al. 2006). The meridional maxima of the SST gradient are allocated to the different ACC fronts. In this context, the very weak surface temperature signal of the SAF in Fig. 3 is interesting, supporting the argument of Boehme et al. (in press) that the SST gradient across the SAF can be very weak in Drake Passage, and suggesting that remotely sensed SST data are not always appropriate for determining the location of the SAF.

Figures 5 and 6 show that the main transport occurs very close to the three main ACC fronts. The transports derived from the high spatial resolution transect of Rudolph show many small current cores, resulting in a much more complex current system than the traditional conceptual model of the ACC frontal system. The high detail of the transports based on the method including shallower depths suggests that these weaker currents only occur in the upper layer. This branching structure of the ACC flow has also been observed in previous work (Moore et al. 1999; Sokolov and Rintoul 2002; Lenn et al. 2007). Previous work using fine-scale sampling techniques in the upper waters of the Southern Ocean has also highlighted

the complex nature of the ACC fronts. Pollard et al. (1995) used a towed undulator to obtain an upper-ocean hydrographic transect upstream of Drake Passage, and observed fine-scale (5–10 km) undulations when crossing the ACC fronts here. Meredith et al. (2003) made similar observations of ''streakiness'' in the SACCF using 2-km resolution data close to South Georgia. This was attributed to differential advection by the ACC fronts, with the large velocities advecting water mass properties along the axis of the front more rapidly than on either side, thus sharpening the cross-frontal gradients. It is believed that this process can lead to phytoplankton patchiness (Pollard et al. 1995), with consequences for the marine ecosystem. We have demonstrated here that in situ fine-scale information on ACC frontal structures is obtainable with the CTD-tagged animals, and without recourse to cruise-based sampling.

In general, the fronts are better resolved in the transect of Rudolph (Fig. 2) than in the data of Jason (Fig. 3) because of the closer station spacing close to the fronts of Rudolph. Rudolph sampled 81 vertical hydrographic profiles with higher station density around the frontal positions. As a result, the horizontal detail of the frontal structures and the detail in transports across Drake Passage are better than analysis on the basis of CTD sections (which typically consists of about 30 profiles), and hence are better able to resolve the fine-scale structures described above. XBT sections commonly have a greater detail, but lack in general salinity measurements. Typically these sections are also preplanned, and so the spatial resolution is the same in the ACC zones as in the fronts, while seals target the fronts preferentially, which gives them great utility when wanting high spatial resolution in regions of rapid change over short distances.

This case shows that southern elephant seals are adaptive samplers, directing sampling effort to particularly interesting and productive regions as they adaptively sample their environment on the basis of previous experience. These foraging areas are also likely to coincide with the regions of most interest to oceanographers. This also has the added benefit that individuals are likely to retrace previous tracks, and can therefore provide repeat sections. Some seal species penetrate deep into polar regions where cloud and partial or near-total sea ice coverage can limit the applicability of oceanographic remote sensing, and where most profiling floats and ships cannot operate (Biuw et al. 2007).

Transports—The maximum transport per unit width above 2,500 m at the position of the three major fronts of the ACC are between 10×10^6 m^3 s^{-1} and 20×10^6 m^3 s^{-1} (Fig. 5). Between the fronts lie regions of weak flow or countercurrents. The transect of Rudolph shows a relatively strong countercurrent of up to 10×10^6 m^3 s^{-1} to the west (Fig. 5) associated with the homogeneous water between the PF and SAF (Fig. 2). The eastward flows associated with the fronts can be distinct as derived from Rudolph or merge as the flow of the PF and SACCF do in the transect of Jason. The total transports of the fronts derived from Fig. 6 are 10–20 $\times$ 10^6 m^3 s^{-1} for the SACCF, 45×10^6 m^3 s^{-1} for the PF, and 10–35 $\times$ 10^6 m^3 s^{-1} for the SAF. This correlates well with the results of previous work (Orsi et al. 1995; Sokolov and Rintoul 2002; Sprintall 2003).

The absolute geostrophic velocity section across Drake Passage at the beginning of April 2005 shows three current cores associated with the three fronts (Fig. 7). A low velocity of about 0.2 m s^{-1} is associated with the SACCF, whereas the PF and SAF show velocities of more than 0.6 m s^{-1}. These surface layer velocities and their vertically coherent structure correlate well with previous findings (e.g., Lenn et al. 2007).

We utilized relationships between upper ocean temperatures and stream functions to determine the cumulative baroclinic transports across Drake Passage on the basis of two methods (Sprintall 2003 and Sokolov et al. 2004). In general, transports $Q_{2,500}$ based on Sprintall (2003) are slightly lower than $\chi_{2,500}$ based on Sokolov et al. (2004) and show more detail. Sprintall (2003) showed that most of the mesoscale variability is only evident in the upper layer above 200 m depth. $Q_{2,500}$ incorporates this variability by including T_{100} and, therefore, shows a higher level of detail. Only by including this upper layer into the estimates are we able to resolve the high frequency variability in Drake Passage.

For the transect of Rudolph in June 2004, we estimate the total baroclinic transport to be 124×10^6 m^3 s^{-1} $\pm$ 14 $\times$ 10^6 m^3 s^{-1}. This agrees well with summertime estimates of previous work. We note, however, that this is an estimate for the total baroclinic wintertime transport through Drake Passage in June 2004 and we lack comparative data. The transect of Jason in April 2005 yields an estimate of 110 $\times$ 10^6 m^3 s^{-1} $\pm$ 14 $\times$ 10^6 m^3 s^{-1}. We assume that this is a low estimate, because of the limited data around the SACCF.

The total transport across Drake Passage in April 2005 in the upper 250 m is estimated at 38×10^6 m^3 s^{-1} $\pm$ 15 $\times$ 10^6 m^3 s^{-1} (Fig. 7). This estimate is higher than the mean transport of 27.8×10^6 m^3 s^{-1} $\pm$ 1 $\times$ 10^6 m^3 s^{-1} between September 1999 and December 2004 of Lenn et al. (2007). Lenn et al. (2007) also report that the upper 250 m accounts for 20% of the total transport. This yields a very high total transport of 190×10^6 m^3 s^{-1} $\pm$ 75 $\times$ 10^6 m^3 s^{-1} derived from the absolute geostrophic field when compared with the total estimate based on the upper ocean temperatures. However, calculating the mean weighted by the variances on the basis of all three transport estimates yields 112 $\times$ 10^6 m^3 s^{-1} $\pm$ 14 $\times$ 10^6 m^3 s^{-1} for April 2005.

In summary, a unique hydrographic data set obtained by instruments attached to two southern elephant seals reveals the frontal structure of the ACC and is analyzed to estimate the total eastward transport in Drake Passage. New technology has enabled us to obtain an in situ data set with high spatial resolution even in the wintertime across Drake Passage. The majority of the uncertainty is due to the accuracy of the sensors. New generations of animal-borne sensors have better sensors and higher accuracy. These high-accuracy sensors have the ability to collect large numbers of profiles cost effectively, particularly at times where traditional oceanographic measurements are scarce. Southern elephant seals are adaptive samplers with increased spatial resolution close to hydrographic fronts

capable of resolving fine-scale structures in the frontal features, and are thus a powerful complement to the existing means of data collection. Future deployments will yield better estimates and provide further detailed information on the locations of the transport changes. These data will be of great benefit in adding to the ship-derived Drake Passage transport estimates, and will help mitigate the seasonal bias in the in situ sampling of the ACC at this location. It is thus of great importance that the CTD-SRDL deployments are maintained and enhanced in number into the future.

References

Belkin, I. M., and A. L. Gordon. 1996. Southern Ocean fronts from the Greenwich meridian to Tasmania. J. Geophys. Res. **101:** 3675–3696, doi:10.1029/95JC02750.

Biuw, M., and others. 2007. Variations in behavior and condition of a southern ocean top predator in relation to in situ oceanographic conditions. Proc. Natl. Acad. Sci. USA **104:** 13705–13710.

Boehme, L., M. P. Meredith, S. E. Thorpe, M. Biuw, and M. Fedak. In press. The ACC frontal system in the South Atlantic: monitoring using merged Argo and animal-borne sensor data. J. Geophys. Res.

Boyd, J. D., and R. Linzell. 1993. The temperature and depth accuracy of Sippican T-5 XBTs. J. Atmos. Ocean. Technol. **10:** 128–136.

Cunningham, S. A., S. G. Alderson, B. A. King, and M. A. Brandon. 2003. Transport and variability of the Antarctic Circumpolar Current in Drake Passage. J. Geophys. Res. **108:** 8084, doi:10.1029/2001JC001147.

Dong, S., J. Sprintall, and S. T. Gille. 2006. Location of the Antarctic Polar Front from AMSR-E Satellite sea surface temperature measurements. J. Phys. Oceanogr. **36:** 2075–2089.

Foster, L. A. 1972. Current measurements in the Drake Passage. Master's thesis, Dalhousie University.

Gille, S. T., and C. W. Hughes. 2001. Aliasing of high-frequency variability by altimetry: Evaluation from bottom pressure recorders. Geophys. Res. Lett. **28:** 1755–1758.

Hughes, C. W., P. L. Woodworth, M. P. Meredith, V. Stepanov, T. Whitworth, and A. R. Pyne. 2003. Coherence of Antarctic sea levels, Southern Hemisphere Annular Mode, and flow through Drake Passage. Geophys. Res. Lett. **30:** 1464, doi:10.1029/2003GL017240.

Lenn, Y.-D., T. K. Chereskin, J. Sprintall, and E. Firing. 2007. Mean jets, mesoscale variability and eddy momentum fluxes in the surface layer of the Antarctic Circumpolar Current in Drake Passage. J. Mar. Res. **65:** 27–58.

Lydersen, C., and others. 2002. Salinity and temperature structure of a freezing Arctic fjord monitored by white whales (*Delphinapterus leucas*). Geophys. Res. Lett. **29:** 2119, doi:10.1029/2002GL015462.

McCarthy, M., L. D. Talley, and D. Roemmich. 2000. Seasonal to interannual variability from XBT and TOPEX/Poseidon data in the South Pacific subtropical gyre. J. Geophys. Res. **105:** 19535–19550, doi:10.1029/2000JC900056.

Meredith, M. P., K. E. Grose, E. L. McDonagh, K. J. Heywood, R. D. Frew, and P. F. Dennis. 1999. Distribution of oxygen isotopes in the water masses of Drake Passage and the South Atlantic. J. Geophys. Res. **104:** 20949–20962, doi:10.1029/98JC02544.

———, and A. M. Hogg. 2006. Circumpolar response of Southern Ocean eddy activity to a change in the Southern Annular Mode. Geophys. Res. Lett. **33:** L16608, doi:10.1029/2006GL026499.

———, and C. Hughes. 2005. On the sampling timescale required to reliably monitor interannual variability in the antarctic circumpolar transport. Geophys. Res. Lett. **32:** L03609, doi:10.1029/2004GL022086.

———, J. L. Watkins, E. J. Murphy, P. Ward, D. G. Bone, S. E. Thorpe, and S. A. Grant. 2003. The southern ACC front to the northeast of South Georgia: Part I. Pathways, characteristics and fluxes. J. Geophys. Res. **108:** 3162.

———, P. L. Woodworth, C. W. Hughes, and V. Stepanov. 2004. Changes in the ocean transport through Drake Passage during the 1980s and 1990s, forced by changes in the Southern Annular Mode. Geophys. Res. Lett. **31:** L21305, doi:10.1029/2004GL021169.

Moore, J. K., M. R. Abbott, and J. G. Richman. 1999. Location and dynamics of the Antarctic Polar Front from satellite sea surface temperature data. J. Geophys. Res. **104:** 3059–3074, doi:10.1029/1998JC00032.

Nowlin, W. D., and M. Clifford. 1982. The kinematic and thermohaline zonation of the antarctic circumpolar current at Drake Passage. J. Mar. Res. **40:** 481–507.

———, and J. M. Klinck. 1986. The physics of the Antarctic Circumpolar Current. Rev. Geophys. **24:** 469–491.

———, T. Whitworth III, and R. D. Pillsburry. 1977. Structure and transport of the Antarctic Circumpolar Current at Drake Passage from short-term measurements. J. Phys. Oceanogr. **7:** 778–802.

Orsi, A. H., T. Whitworth III, and W. D. Nowlin. 1995. On the meridional extent and fronts of the Antarctic Circumpolar Current. Deep-Sea Res. I **42:** 641–673.

Piola, A. R., and A. L. Gordon. 1989. Intermediate waters in the southwest South Atlantic. Deep-Sea Res. A **36:** 1–16.

Pollard, R., J. F. Read, J. T. Allen, G. Griffiths, and A. I. Morrison. 1995. On the physical structure of a front in the Bellingshausen Sea. Deep-Sea Res. II **42:** 955–982.

Reid, J. L., and W. D. Nowlin. 1971. Transport of water through the Drake Passage. Deep-Sea Res. **18:** 51–64.

Ridgway, K., and J. S. Godfrey. 1994. Mass and heat budgets in the East Australian Current: A direct approach. J. Geophys. Res. **99:** 3231–3248, doi:10.1029/93JC02255.

Rintoul, S. R., J. R. Donguy, and D. H. Roemmich. 1997. Seasonal evolution of upper ocean thermal structure between Tasmania and Antarctica. Deep-Sea Res. I **44:** 1185–1202.

———, C. W. Hughes, and D. Olbers. 2001. The Antarctic Circumpolar Current system, p. 271–302. *In* G. Siedler, J. Church and J. Gould [eds.], Ocean circulation and climate: Observing and modelling the global ocean. Academic Press.

———, S. Sokolov, and J. A. Church. 2002. A 6 year record of baroclinic transport variability of the Antarctic Circumpolar Current at 140E derived from XBT and altimeter measurements. J. Geophys. Res. **107:** 3155, doi:10.1029/2001JC000787.

Rio, M.-H., and F. Hernandez. 2004. A mean dynamic topography computed over the world ocean from altimetry, in situ measurements, and a geoid model. J. Geophys. Res. **109:** C12032, doi:10.1029/2003JC002226.

Sokolov, S., B. A. King, S. R. Rintoul, and R. L. Rojas. 2004. Upper ocean temperature and the baroclinic transport stream function relationship in Drake Passage. J. Geophys. Res. **109:** C05001, doi:10.1029/2003JC002010.

———, and S. R. Rintoul. 2002. Structure of Southern Ocean fronts at 140°E. J. Mar. Syst. **37:** 151–184.

SPRINTALL, J. 2003. Seasonal to interannual upper-ocean variability in the Drake Passage. J. Mar. Res. **61:** 25–57.

SSALTO/DUACS USER HANDBOOK. 2006. (M)SLA and (M)ADT near-real time and delayed time products, SALP-MU-P-EA-21065-CLS. Toulouse, France.

TALLEY, L. D. 1996. Antarctic intermediate water in the South Atlantic, p. 219–238. *In* G. Wefer, W. H. Berger, G. Siedler and D. Webb [eds.], The South Atlantic: Present and past circulation. Springer-Verlag.

THOMPSON, D. W. J., AND S. SOLOMON. 2002. Interpretation of recent Southern Hemisphere climate change. Science **296:** 895–899.

———, AND J. M. WALLACE. 2000. Annular modes in the extratropical circulation. Part I: Month-to-month variability. J. Clim. **13:** 1000–1016.

WHITWORTH, T. 1983. Monitoring the transport of the Antarctic Circumpolar Current at Drake Passage. J. Phys. Oceanogr. **13:** 2045–2057.

———, AND R. G. PETERSON. 1985. Volume transport of the Antarctic Circumpolar Current from bottom pressure measurements. J. Phys. Oceanogr. **15:** 810–816.

Received: 6 September 2007
Accepted: 11 December 2007
Amended: 25 December 2007